

# Evidence for the dynamical dark energy with evolving Hubble constant

Yi-Ying Wang<sup>1</sup>, Yin-Jie Li<sup>1</sup>, and Yi-Zhong Fan<sup>1,2,\*</sup>

<sup>1</sup> Key Laboratory of Dark Matter and Space Astronomy, Purple Mountain Observatory, Chinese Academy of Sciences, Nanjing 210033, People's Republic of China

<sup>2</sup> School of Astronomy and Space Science, University of Science and Technology of China, Hefei, Anhui 230026, People's Republic of China

Received December 09, 2025

## ABSTRACT

**Context.** Hubble constant tension, together with the recent indications of dynamical dark energy proposed from the Dark Energy Spectroscopic Instrument (DESI) baryon acoustic oscillation (BAO) measurements, poses significant challenges to the standard cosmological model.

**Aims.** We investigate the possible redshift evolution of dark energy and the Hubble constant through a data-driven approach, and assess whether such evolution can alleviate the Hubble constant tension.

**Methods.** We perform a model-independent reconstruction of the dark-energy equation of state  $w(z)$ , jointly with an evolving Hubble constant  $H_0(z)$ . The analysis combines the DESI DR2 BAO dataset with multiple Type Ia supernova samples and evaluates the statistical preference for the reconstructed model using Bayesian evidence.

**Results.** The reconstructed  $w(z)$  varies with redshift and exhibits two potential phantom crossings at  $z \sim 0.5$  and  $z \sim 1.5$ . Meanwhile,  $H_0$  decreases continually from local to high redshift, alleviating the Hubble constant tension effectively. The joint  $w(z)$ - $H_0(z)$  model is favored over the  $w$ CDM ( $\Lambda$ CDM) framework, with a logarithmic Bayes factor  $\ln \mathcal{B} = 5.04$  (8.53). The results remain stable under different prior choices and dataset combinations.

**Conclusions.** Our data-driven reconstructions suggest redshift evolution in both  $w(z)$  and  $H_0(z)$ , offering a potential route to mitigate the Hubble constant tension. Future BAO measurements from Euclid and next-generation CMB experiments will provide critical tests of these results and bring deeper insights into the nature of dark energy and the evolution of cosmic expansion.

**Key words.** cosmological parameters – dark energy

## 1. Introduction

The standard cosmological paradigm, the cosmological constant  $\Lambda$  and the Cold Dark Matter ( $\Lambda$ CDM) model, successfully explains most cosmological observations. However, the Hubble constant tension and possible evidence for dynamical dark energy pose significant challenges to this standard cosmological framework (Perivolaropoulos & Skara 2022; Abdalla et al. 2022; Di Valentino & Brout Dillon 2024; Di Valentino et al. 2025; Wang et al. 2026). Combining Cepheid-based distance measurements from the James Webb Space Telescope (JWST) and the Hubble Space Telescope (HST), Riess et al. (2025) reported a local Hubble constant of  $H_0 = 73.8 \pm 0.88 \text{ km s}^{-1} \text{ Mpc}^{-1}$  via the distance-ladder method (Riess et al. 2021, 2022), which deviates from the  $\Lambda$ CDM prediction inferred from the cosmic microwave background (CMB) (Planck Collaboration et al. 2020) at the  $\sim 6\sigma$  confidence level. Meanwhile, the recent Baryon acoustic oscillation (BAO) measurements from the Dark Energy Spectroscopic Instrument (DESI) Data Release 2 (DR2) (DESI Collaboration et al. 2025) prefer a dynamical dark energy model with CPL parameterization over  $\Lambda$ CDM at a  $2.8 - 4.2\sigma$  confidence level when combined with CMB and type Ia supernovae (SNe Ia) data. A  $\sim 5\sigma$  level tension has been reported by Scherer et al. (2025) when adopting different parameterization for  $w(z)$ .

Both the Hubble constant and dark energy govern the accelerating expansion of the Universe, describing its local expansion rate and the physical mechanism behind cosmic acceleration. The dark-energy equation of state (EoS),  $w \equiv P/c^2\rho$ , serves as a crucial diagnostic:  $w = -1$  corresponds to vacuum energy within  $\Lambda$ CDM model. For dynamical dark energy,  $w$  evolves with time and can be categorized into various models according to their trajectories in the  $w$  phase space, including quintessence (Ratra & Peebles 1988), phantom (Caldwell 2002), quintom (Feng et al. 2005),  $k$ -essence (Armendariz-Picon et al. 2000) and others. For the phenomenological quintom model (Feng et al. 2006), an oscillating evolution of  $w(z)$  naturally arises, accompanied with a varying  $H_0$ . Several studies suggest that late-time transitions in dark energy could alleviate the Hubble tension by reducing local  $H_0$  values (Benevento et al. 2020; Di Valentino et al. 2021; Pang et al. 2025). However, combining the latest DESI DR2 BAO and CMB data, a lower Hubble constant  $H_0 = 63.7^{+1.7}_{-2.2} \text{ km s}^{-1} \text{ Mpc}^{-1}$  was obtained (DESI Collaboration et al. 2025), thereby exacerbating the Hubble tension. Furthermore, whether current data provide robust evidence for dynamical dark energy remains an open question (Giarè 2025; Ó Colgáin & Sheikh-Jabbari 2025).

To reconcile the discrepancies in Hubble constant measurements between early- and late-time cosmological observations, several studies have constrained  $H_0$  by dividing the data into redshift bins. Wong et al. (2020) first reported an appar-

\* Corresponding author: yzfan@pmo.ac.cn

ent trend of decreasing  $H_0$  inferred from the individual lensing systems. A possible dynamical evolution of  $H_0$  has since been investigated using a phenomenological function (Dainotti et al. 2021, 2022, 2025), modified definitions of the Hubble constant (Krishnan et al. 2021; Jia et al. 2025b), and direct binned measurements (Krishnan et al. 2020; Malekjani et al. 2024; Ó Colgáin et al. 2024; Lopez-Hernandez & De-Santiago 2025). Similarly, the EoS of dark energy  $w(z)$  has been widely reconstructed in redshift bins without imposing an explicit functional form (Zhao et al. 2012, 2017; Abedin et al. 2025). Evidences for the oscillations in  $w(z)$  have been found using non-parametric and analytical approaches (Gu et al. 2025; Goldstein et al. 2025), respectively. Given the unknown essence of dark energy remains, such non-parametric, data-driven approaches provide a robust way to trace the evolution of  $w(z)$ .

In this work, we simultaneously investigate a model-independent dynamical dark energy and an evolving Hubble constant for the first time. We do not assume any specific forms for the dark energy and  $H_0$ , but instead reconstruct both functions directly from the data using a data-driven approach. The datasets we use include the DESI DR2 BAO measurements (DESI Collaboration et al. 2025), SNe Ia observations from the PantheonPlus compilation (Brout et al. 2022; Scolnic et al. 2022), the five-year Dark Energy Survey sample (DESY5) (DES Collaboration et al. 2024), and the Union3 compilation (Rubin et al. 2025). Without assuming any specific functional form, we employ Gaussian process to reconstruct  $w(z)$  and  $H_0(z)$  over the redshift range of  $0 < z < 2.5$ . The values of  $w$  and  $H_0$  are sampled in each redshift bin, enabling a complementary analysis that balances model flexibility and constraining power.

## 2. Methods

Considering a flat universe ( $\Omega_K = 0$ ), the expansion rate is

$$\frac{H(z)}{H_0(z)} = [\Omega_m(1+z)^3 + \Omega_{DE} \frac{\rho_{DE}(z)}{\rho_{DE,0}}]^{1/2}, \quad (1)$$

where  $\Omega_m$ ,  $\Omega_{DE}$  are the present-time matter and dark energy density parameters, respectively, and  $H_0(z)$  represents the Hubble parameter evaluated in the corresponding-redshift bin. Here,  $H_0(z)$  can be regarded as an effective, redshift-dependent normalization of the expansion rate, rather than a fundamental Hubble constant. As shown in Krishnan et al. (2021), the Hubble constant can be represented as an integration constant from the Friedmann equation within the FLRW cosmology. Therefore, Equation 1 reduces to the FLRW framework only when  $H_0(z)$  is a constant. The energy density  $\rho_{DE}$  that normalized to its present value evolves as

$$\frac{\rho_{DE}(z)}{\rho_{DE,0}} = \exp \left[ 3 \int_0^z [1 + w(z)] \frac{dz'}{1 + z'} \right]. \quad (2)$$

The contributions from radiation and massive neutrinos are neglected for simplification. The BAO distance observables include the comoving distance  $D_M(z)$ , the Hubble distance  $D_H(z)$ , and the angle-average distance  $D_V(z)$ , which can be written as

$$\begin{aligned} D_M(z) &= \int_0^z \frac{c dz'}{H(z')}, \\ D_H(z) &= \frac{c}{H(z)}, \end{aligned} \quad (3)$$

and  $D_V(z) = (z D_M(z)^2 D_H(z))^{1/3}$ .

The pre-recombination sound horizon at the drag epoch is defined as  $r_d = \int_{z_d}^{\infty} c_s(z)/H(z) dz$ , where  $c_s$  is the sound speed in the primordial plasma. Following Brieden et al. (2023) and DESI Collaboration et al. (2025), it can be approximated as

$$r_d = 147.05 \text{ Mpc} \times \left( \frac{\Omega_b h^2}{0.02236} \right)^{-0.13} \left( \frac{\Omega_m h^2}{0.1432} \right)^{-0.23} \left( \frac{N_{\text{eff}}}{3.04} \right)^{-0.1}, \quad (4)$$

where  $h \equiv H_{0,z=0}/(100 \text{ km s}^{-1} \text{ Mpc}^{-1})$  and  $N_{\text{eff}}$  is the effective number of neutrino species. In this work, only the variations in  $\Omega_b$  and  $\Omega_m$  are considered. The DESI DR2 BAO data cover  $0.1 < z < 4.2$  using multiple tracers: the bright galaxy sample ( $0.1 < z < 0.4$ ), luminous red galaxies ( $0.4 < z < 1.1$ ), emission line galaxies ( $1.1 < z < 1.6$ ), quasars ( $0.8 < z < 2.1$ ) and Ly $\alpha$  forest ( $1.77 < z < 4.16$ ). For the SNe Ia samples, the Pantheon-Plus compilation<sup>1</sup> (Brout et al. 2022; Scolnic et al. 2022) contains 1701 light curves of 1550 distinct SNe Ia covering  $0.001 < z < 2.26$ , the DESY5 sample (DES Collaboration et al. 2024) includes 1635 SNe Ia within  $0.10 < z < 1.13$ , and the Union3 compilation<sup>2</sup> (Rubin et al. 2025) provides 2087 SNe Ia covering  $0.001 < z < 2.26$ . We use the observations that satisfy  $z > 0.01$ . The luminosity distance is given by  $D_L(z) = (1+z)D_M(z)$ .

We model the evolution of  $w(z)$  and  $H_0(z)$  over the redshift range  $0 < z < 2.5$ . The upper bound of  $z = 2.5$  is a conservative choice that encompasses all the observational datasets used in this analysis. The target range is divided into 29 bins of uniform width in scale factor ( $a = 1/(1+z)$ ) space (Gu et al. 2025). To reconstruct smooth and continuous functions of  $w(z)$  and  $H_0$  without assuming any explicit functional form, we employ Gaussian Process (GP) as a non-parametric statistical method. GP has been extensively applied in data-driven astronomy (Holsclaw et al. 2010; Shafieloo et al. 2012; Li et al. 2021), demonstrating powerful strength to sample the space of continuous functions. For prior assumptions, we adopt three types of kernels/methods to construct the covariance matrices  $\Sigma$ : the Matérn kernel  $K_{\text{Matérn}}(\delta a, \nu, l)$ , Gaussian kernel  $K_{\text{Gaussian}}(\delta a, l)$  and Horndeski theory (Horndeski 1974). The general form of the covariance matrix is  $\Sigma_{ij} = \sigma^2 K(|a_i - a_j|, l)$ , where  $\sigma$  represents the amplitude of the function,  $a_i$  denotes the median point of the  $i$ -th bin in scale factor space, and  $l$  governs the correlation length scale. For the Horndeski-based covariance, we adopt the prior covariance from Horndeski-based simulations (Raveri et al. 2017), expressed as

$$\begin{aligned} C(a_i, a_j) &= \sqrt{C(a_i)C(a_j)}R(a_i, a_j), \\ C(a_i) &= 0.05 + 0.8a_i^2, \\ R(a_i, a_j) &= \exp[-(|\ln a_i - \ln a_j|/0.3)^{1.2}]. \end{aligned} \quad (5)$$

Following Gu et al. (2025), the covariance matrix  $\Sigma$  is calculated as

$$\Sigma = [(\mathbf{I} - \mathbf{S})^T \mathbf{C}^{-1} (\mathbf{I} - \mathbf{S})]^{-1}, \quad (6)$$

where  $\mathbf{I}$  is the identity matrix and  $\mathbf{S}$  is the transformation matrix that averages over 5 neighboring  $w$  bins. The Horndeski-based covariance matrix predicts a variable  $\sigma(w)$  ranging from 1.6 to 6.2 across bins. Accordingly, we adopt a constant  $\sigma(w) = 3$

<sup>1</sup> We use the PantheonPlus compilation accompanied by the SH0ES Cepheids, obtained from <https://github.com/PantheonPlusSH0ES/>

<sup>2</sup> The likelihoods of the DESY5 and Union3 compilations are calculated by the cosmological inference software `cobaya` (<https://github.com/CobayaSampler>).

for both the Matérn and Gaussian kernels, in order to ensure a consistent comparison across different kernel and model assumptions. For the  $H_0(z)$  reconstruction, we set  $\sigma(H_0) = 15$  as a weakly informative prior in the Bayesian inference, ensuring that the reconstructed evolution of  $H_0(z)$  is driven primarily by the data rather than by prior assumptions. The mean values are assumed to be  $\mu(H_0) = 70$  and  $\mu(w) = -1$ , respectively. In this work, it should be noticed that Gaussian processes are employed as functional priors on  $w(z)$  and  $H_0(z)$ , rather than as a direct interpolation technique. The correlation length  $l$  is not optimised by maximizing or marginalizing GP likelihoods. Instead, we scan a range of fixed values and asses their performance by comparing the Bayesian evidence of the full cosmological model. We apply a flat prior on  $\Omega_m$  and a Gaussian prior on  $\Omega_b$ , with  $\Omega_m \in [0.1, 0.5]$  and  $\Omega_b h^2 = 0.02196 \pm 0.00063$  (Schöneberg 2024). Additional constrains require  $H_0(z)$  and  $w(z)$  remain within  $[50, 90]$  and  $[-6, 4]$ , respectively.

Since all of the components involved in the DESI BAO and SNe Ia measurements have been explicitly implemented, the likelihood functions in the Bayesian statistical framework can be written as

$$\begin{aligned} \mathcal{L}_{\text{BAO}} &= \prod_i^N \exp \left[ -\frac{1}{2} \left( \frac{f(x_i) - y_i}{\sigma_i} \right)^2 \right], \\ \mathcal{L}_{\text{SNe}} &= \exp \left[ -\frac{1}{2} \Delta \mathbf{D}^T C_{\text{stat+syst}}^{-1} \Delta \mathbf{D} \right], \end{aligned} \quad (7)$$

where  $(x_i, y_i)$  and  $\sigma_i$  are the DESI BAO measurements and their uncertainties,  $\mathbf{D}$  is the vector of SNe Ia distance modulus residuals, defined as  $\Delta D_i = \mu_i - \mu_{\text{model}}(z_i)$ , and  $C_{\text{stat+syst}}$  denotes the statistical and systematic covariance matrices. To balance the efficiency and accuracy, we employ the nested sampling algorithm implemented in `pymultinest` (Buchner 2016) and set 2000 live points during Bayesian analysis.

### 3. Results

The evolutions of  $w(z)$  and  $H_0(z)$  are reconstructed simultaneously. Each is divided into 29 bins. The priors of  $\mathbf{w} = (w_1, \dots, w_{29})$  and  $\mathbf{H}_0 = (H_{0,1}, \dots, H_{0,29})$  are generated either from the Horndeski theory or from the GP kernel functions, expressed as  $\pi(\mathbf{w}|\mu, \sigma, l)$  and  $\pi(\mathbf{H}_0|\mu, \sigma, l)$ , respectively. Besides  $\sigma$ , the length scale  $l$  acts as another hyper parameter that regulates the smoothness of reconstructed functions. Larger  $l$  values enforce stronger correlations, stiffening the model that will ignore the details, while smaller  $l$  values soften the model but may risk overfitting. We compare Bayesian evidences across several configurations with different  $l$  values and find that  $H_0(z)$  shows a clear decreasing trend. This preference for a smoother function for  $H_0(z)$  leads us to adopt a Gaussian kernel with a relatively large length scale. Detailed comparisons of the scale length are provided in section 4.

Figure 1 illustrates the reconstructed  $w(z)$  (top panels) and  $H_0(z)$  (bottom panels) derived from various data combinations. The priors of  $\mathbf{w}$  are generated using the Matérn-3/2 kernel with  $l = 2.5$  and  $\nu = 2/3$  for the DESI + PantheonPlus and DESI + DESY5 datasets, and  $l = 0.9$  for the DESI + Union3 case. The priors of  $\mathbf{H}_0$  are generated using the Gaussian kernel with  $l = 2.0$ . These configurations yield the highest Bayesian evidence among all tested  $l$  values, rather than being fitted through a Gaussian process or marginal likelihood optimization. In all cases,  $w(z)$  exhibits clear redshift evolution with multiple peaks, while  $H_0(z)$  demonstrates a significant decreasing trend from

$\sim 73$  to  $\sim 70 \text{ km s}^{-1} \text{ Mpc}^{-1}$ , approaching the CMB-inferred value. To quantify the model preference for dynamical dark energy and an evolving Hubble constant, we compute the Bayes factor,  $\mathcal{B} = \frac{P(y|\mathcal{M}_{w+H_0(z)})}{P(y|\mathcal{M}_w \text{ CDM})}$ . The priors of the  $w$ CDM model are consistent with those described previously. From left to right in Figure 1, we obtain  $\ln \mathcal{B} = 4.18, 3.39$ , and  $2.13$ , respectively. Compared with  $\Lambda$ CDM models, Bayes factors give  $\ln \mathcal{B} = 0.69, 7.67$ , and  $1.54$ , respectively. As pointed out by Jeffreys (1939),  $\ln \mathcal{B} > 2.3$  ( $\ln \mathcal{B} > 3.5$ ) indicates a strong (very strong) preference for one model over another, and  $\ln \mathcal{B} > 4.6$  is regarded as decisive evidence. Thus, the DESI + PantheonPlus and DESI + DESY5 datasets provide a very strong and strong support for the joint  $w(z)$ - $H_0(z)$  model.

As a robustness test, the results using Gaussian kernels and Horndeski theory are shown in Figure 2 and Figure 3, respectively. The priors of  $\mathbf{H}_0$  are generated using the Gaussian kernel with  $l = 2.0$ , except for the middle and right panels in Figure 3, which use a Gaussian kernel with  $l = 1.0$ . The Gaussian kernel yields smoother reconstructions with larger length scale, whereas the Matérn kernel allows greater flexibility. The Horndeski prior produces the most flexible  $w(z)$  evolution, capturing more distinct features in the observations. In Figure 2, the blue regions corresponds that the priors of  $w$  are generated by Gaussian kernel with  $l = 0.2$  for DESI + PantheonPlus and DESI + DESY5, and  $l = 0.05$  for DESI + Union3 scenarios. The resulting Bayes factors relative to  $w$ CDM ( $\Lambda$ CDM) model are  $\ln \mathcal{B} = 3.74$  (0.23),  $2.96$  (7.24), and  $2.86$  (2.27), respectively, again showing very strong preference for DESI + PantheonPlus and strong preference for other datasets. The purple regions in the right panels represent reconstructions with  $l = 0.2$ , yielding consistent shapes compared with other scenarios using different datasets but a smaller  $\ln \mathcal{B} = 0.64$ . For the results using the Horndeski prior shown in Figure 3, Bayes factors relative to  $w$ CDM ( $\Lambda$ CDM) model are  $\ln \mathcal{B} = 5.04$  (1.55),  $4.25$  (8.53), and  $3.06$  (2.47) for differ datasets, respectively. Notably, the DESI + PantheonPlus combination provides a decisive evidence ( $\ln \mathcal{B} > 4.6$ ) favoring the  $w(z)$ - $H_0(z)$  model.

All nine scenarios, constructed with different dataset combinations and prior assumptions, consistently indicate that both the dark-energy EoS  $w(z)$  and the Hubble constant  $H_0$  can evolve with redshift. Compared with Equation 1 and Equation 2, the evolved  $H_0$  suggests that dynamical dark energy alone may not be sufficient to fully explain the Hubble constant tension, potentially indicating the presence of new physics beyond the standard cosmological model. Several deviations from  $\Lambda$ CDM model appear at distinct epochs. The reconstructed  $w(z)$  crosses into the phantom regime ( $w < -1$ ) around  $z \approx 0.5$ , consistent with previous non-parametric DESI BAO analyses (Lodha et al. 2025). It returns to the quintessence regime around  $z \approx 1.0$ , and then crosses again into the phantom region near  $z \approx 1.5$ . Particularly, all reconstructions show a preference for  $w(z)$  exhibiting two phantom crossings. Furthermore, no clear non-monotonic behavior is observed in  $H_0(z)$ . Instead, all results present a gradual decline from local to higher redshift, with different amplitudes depending on the dataset and prior choice. The DESI + PantheonPlus case with Gaussian kernel yields the smallest variation, from  $73.11^{+0.90}_{-0.85}$  to  $71.60^{+1.27}_{-1.26} \text{ km s}^{-1} \text{ Mpc}^{-1}$ , while the DESI + DESY5 case with Horndeski theory gives the largest one, from  $75.81^{+3.39}_{-2.53}$  to  $67.41^{+1.36}_{-1.12} \text{ km s}^{-1} \text{ Mpc}^{-1}$ . Compared with the results based on the classical CPL parameterization (DESI Collaboration et al. 2025), a lower  $H_0$  value is typically obtained when  $w_0 > -1$ , as a consequence of parameter degeneracy inherent in the CPL model (Lee et al. 2022). Differ-

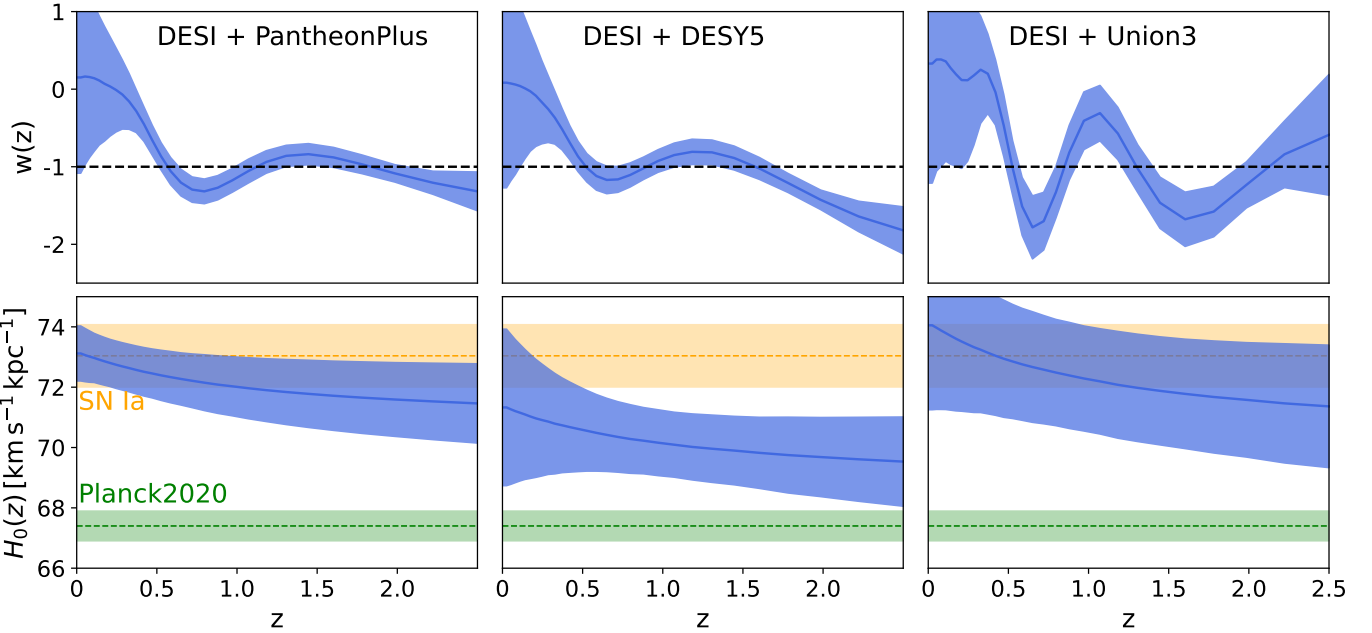


Fig. 1: Reconstructed dark-energy EoS  $w(z)$  and Hubble constant  $H_0(z)$  from multiple datasets. The GP priors for  $w(z)$  and  $H_0(z)$  use Matérn-3/2 and Gaussian kernels, respectively. Panels in each column correspond to using the same datasets. Solid blue lines show the mean values of the  $w(z)$  and  $H_0(z)$  distributions. The shaded blue regions indicate the corresponding 68% credible intervals. The dashed black lines marks  $w = -1$ . The orange and green bands denote  $H_0$  estimations from SNe Ia (Riess et al. 2022) and CMB (Planck Collaboration et al. 2020).

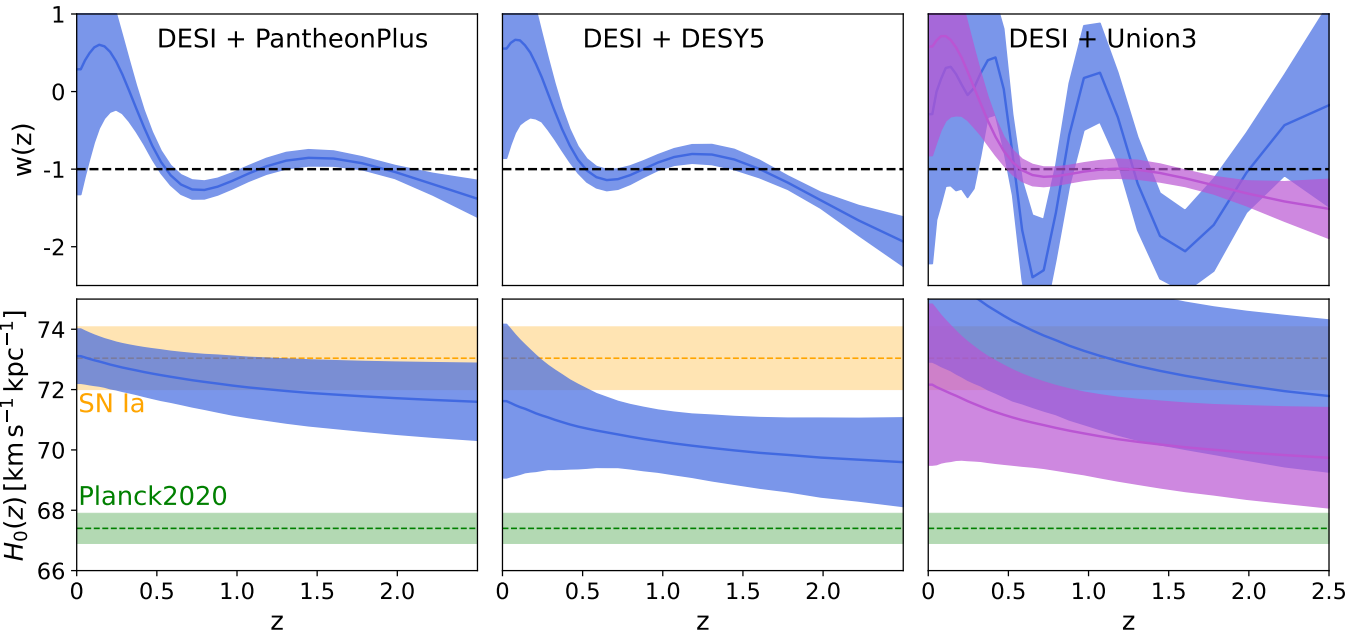


Fig. 2: Similar to Figure 1, but showing the posterior reconstruction of  $w(z)$  obtained by adopting a Gaussian kernel to define the GP prior covariance. In the right panel, the blue region represents the results with a maximum Bayes factor with  $l = 0.05$ . The purple region corresponds to  $l = 0.2$ , assuming the same scale length as in the left and middle panels. A smaller  $l$  ( $l < 0.01$ ) in the DESI + Union case may yield a higher Bayesian evidence, but the resulting  $w(z)$  becomes too flexible to provide clear constraint. Therefore, the right panel only shows the results for  $l = 0.05$  and  $l = 0.2$ .

ently, our result alleviates the Hubble constant tension through the downward evolution of  $H_0(z)$ , enabled by a dynamical dark energy with greater freedom than the CPL parameterization.

#### 4. Conclusions and discussions

In this work, we reconstruct the dynamical dark-energy EoS  $w(z)$  together with an evolving Hubble constant  $H_0(z)$  by non-

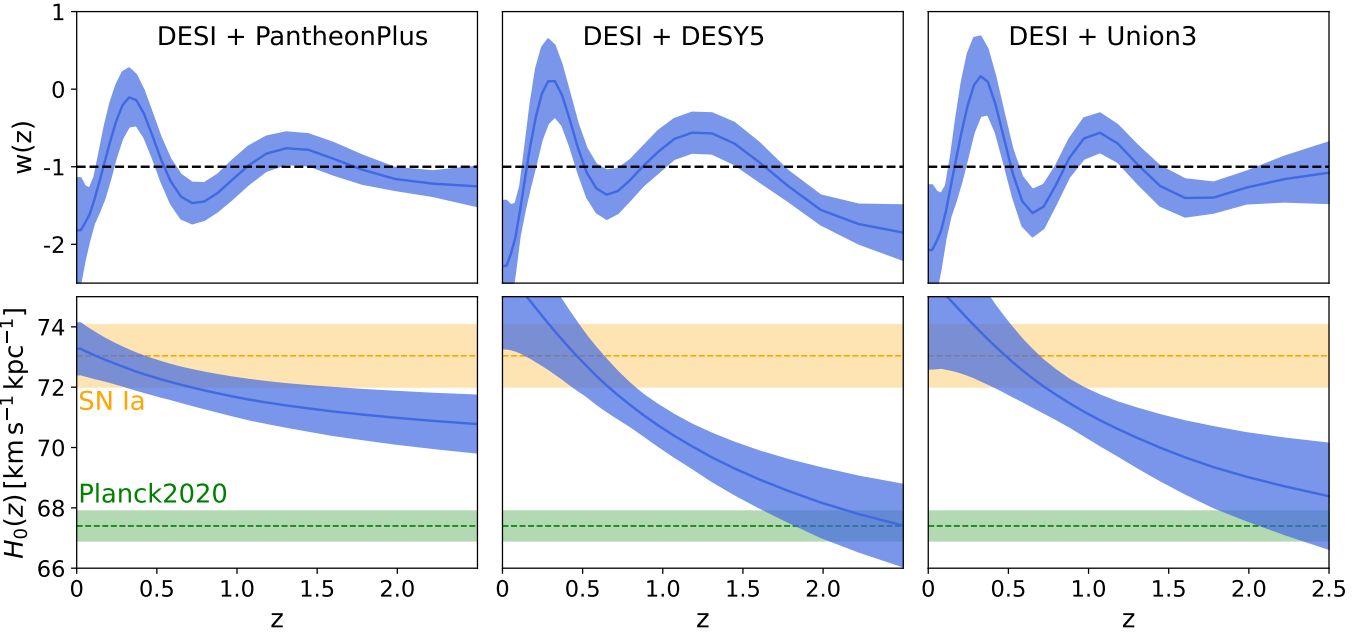


Fig. 3: Similar with Figure 1, but using the Horndeski theory to derive the  $w(z)$  prior. The results in the left panel use a Gaussian kernel with  $l = 2.0$  to derive the  $H_0(z)$  priors, while the others use  $l = 1.0$  to obtain the maximum Bayes factors.

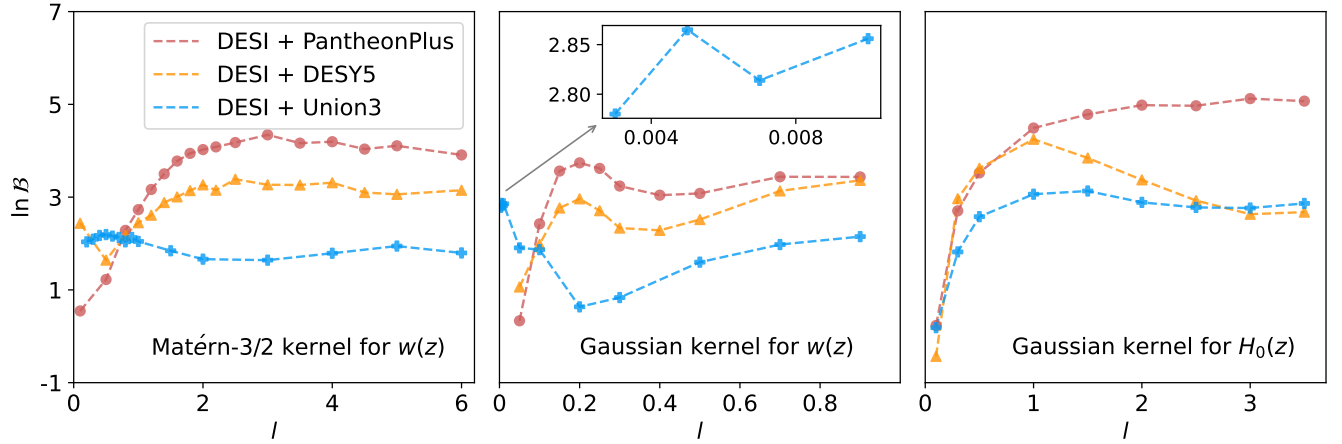


Fig. 4: Comparisons with different scale length under various prior assumptions. The red, orange, and blue scatters represent the Bayes factors relative to  $w\text{CDM}$  models using DESI combined with PantheonPlus, DESY5, and Union3 datasets, respectively.

parametric methods. Across multiple dataset combinations and prior assumptions, we find consistent evolution patterns:  $w(z)$  evolves with redshift and emerges two potential phantom crossing, and  $H_0(z)$  decreases smoothly toward high redshift. In particular, the DESI + DESY5 scenario with the Horndeski prior gives the largest downward,  $\Delta H_0 \sim 8.4 \text{ km s}^{-1} \text{ kpc}^{-1}$ , reaching  $H_0 \sim 67.4 \text{ km s}^{-1} \text{ Mpc}$ . Compared with  $w\text{CDM}$  model and  $\Lambda\text{CDM}$  model ( $w = -1$ ), the Bayes factors are  $\ln \mathcal{B} = 4.25$  and 8.53, respectively, providing a promising solution to relieve the Hubble constant tension. Furthermore, the maximum Bayes factor among all scenarios compared with  $w\text{CDM}$  model reaches  $\ln \mathcal{B} = 5.04$ , establishing decisive evidence for  $w(z)$ - $H_0(z)$  model.

The above results and discussions depend on the choice of the characteristic scale length  $l$ . To clarify the selection of  $l$  in each case, we compare the Bayes factors relative to the  $w\text{CDM}$

model for different scale factor  $l$  across multiple scenarios. As shown in Figure 4, the panels from left to right display the variations of  $\ln \mathcal{B}$  in the reconstructions of  $w(z)$  using Matérn-3/2 and Gaussian kernels, and of the  $H_0(z)$  using Gaussian kernels. In the left and middle panels, the priors of  $H_0(z)$  are generated with a Gaussian kernel of  $l = 2.0$ , while in the right panel, the priors of  $w(z)$  are derived from the Horndeski theory and the priors of  $H_0(z)$  are constructed with a Gaussian kernel using variable  $l$ . The variations of  $\ln \mathcal{B}$  in the middle panel exhibit a moderate increase with larger  $l$ , which may result from the reduced effective degrees of freedom introduced by smoother Gaussian-kernel priors. The maximum values of  $\ln \mathcal{B}$  correspond to the results presented in section 3. Detailed parameter estimation results are listed in Appendix A.

Given that the measurements of BAO relies on the pre-recombination sound-horizon scale and the degeneracy between

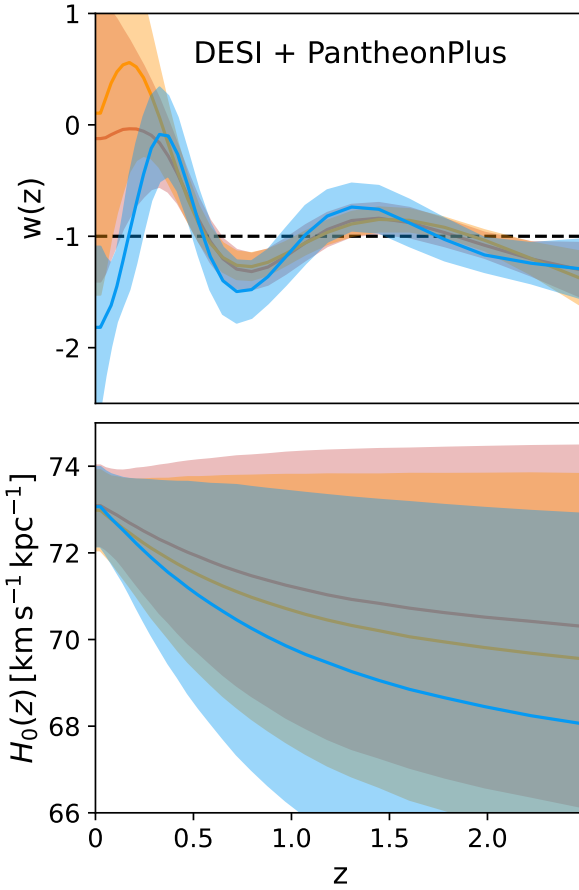


Fig. 5: The reconstructions of  $w(z)$  and  $H_0(z)$  using the DESI + PantheonPlus datasets. The prior of  $H_0(z)$  uses the Gaussian kernel with  $l = 1.5$ . The shaded regions indicate the corresponding 68% credible intervals. The red, orange and blue regions correspond to  $w(z)$  priors generated from the Matérn-3/2 kernel ( $l = 2.5$ ), the Gaussian kernel ( $l = 0.2$ ), and the Horndeski theory, respectively.

$r_d$  and  $H_0$ , we examine the impact of  $r_d$  on the constructions of  $w(z)$  and  $H_0(z)$ . Instead of adopting the fixed relation in Equation 4, we assume  $r_d$  to be a free parameter with a uniform prior of  $[120, 180]$  Mpc. Figure 5 shows the results using the DESI + PantheonPlus datasets. The reconstructed  $w(z)$  remains consistent with previous cases, and  $H_0(z)$  continues to exhibit the same decreasing trend. As expected, the uncertainties in  $H_0(z)$  increase because BAO measurements constrain the product  $H_0 r_d$  more tightly than the individual parameters (DESI Collaboration et al. 2025). For example, under the Horndeski prior,  $H_0$  declines from  $73.06^{+0.92}_{-0.91}$  to  $68.04^{+4.86}_{-3.65}$   $\text{km s}^{-1} \text{kpc}^{-1}$ . Three different prior assumptions are used, including the Matérn-3/2 kernel, the Gaussian kernel with  $l = 0.2$ , and the Horndeski theory. The Bayes factors relative to the  $w\text{CDM}$  model are  $\ln \mathcal{B} = 3.17, 2.66$ , and  $4.02$ , respectively, corresponding to two strong and one very strong preference for the  $w(z)$ - $H_0(z)$  framework.

The reconstruction of  $w(z)$  using both Matérn-3/2 and Gaussian kernels shows consistent results with the Horndeski prior, particularly the evidence of two phantom crossings. Based on independent analyses, Gu et al. (2025) and Goldstein et al. (2025) have reported oscillatory features in  $w(z)$  consistent with our results. To validate the reconstruction method, we perform the same procedure using the simulated data with observational uncertainties matching those of PantheonPlus and DESI DR2. As

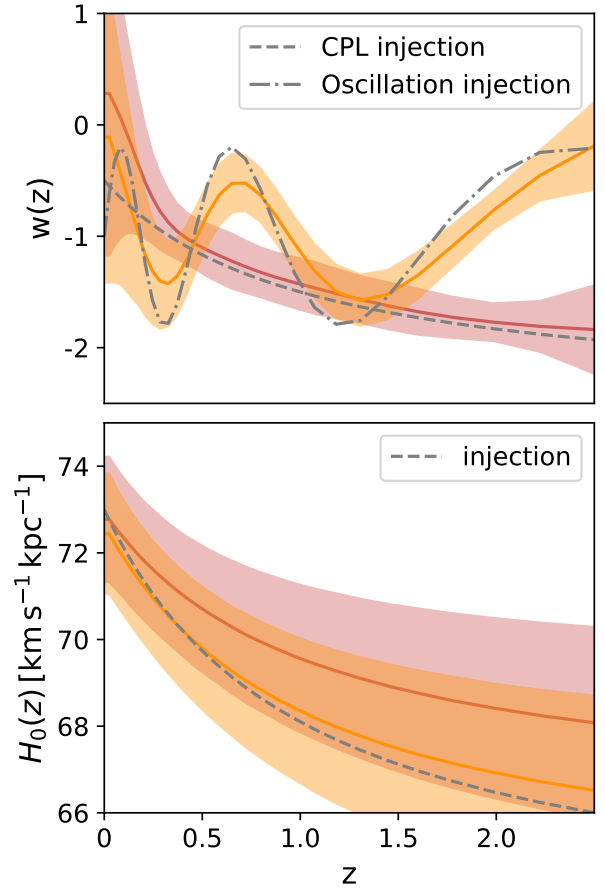


Fig. 6: The reconstructions of  $w(z)$  and  $H_0(z)$  based on simulated injection. The grey lines denote the injected models. For  $w(z)$ , the dashed grey line represents the CPL parameterization with  $w(z) = -0.5 - 2(1 - 1/(1 + z))$  and the dash-dot grey line shows the oscillation model with  $w(z) = 0.8 \sin[20(1 - 1/(1 + z))] - 1$ . For simplicity, the other injected parameters are fixed with  $\Omega_m = 0.3$ ,  $\omega_b h^2 = 0.02196$ , and  $M_b = -19.5$ . For  $H_0(z)$ , the dashed grey line corresponds  $H_0(z) = 73 - 9.8(1 - 1/(1 + z))$ . The shaded regions indicate the corresponding 90% credible intervals. The prior of  $H_0(z)$  uses the Gaussian kernel with  $l = 2.0$ , and the prior of  $w(z)$  is generated from the Matérn-3/2 kernel ( $l = 2.5$ ).

shown in Figure 6, both the CPL parameterization and the oscillation model can be accurately reconstructed using the same kernel function. For the scenario using the CPL parameterization, no pseudo oscillation arise, demonstrating the robustness of our method and the reliability of the physical transition signatures identified in our results.

As one of the most general scalar-tensor theories involving second-order field equations, the Horndeski framework has been widely investigated for its potential to alleviate the Hubble tension by predicting a large  $H_0$  (Petronikolou et al. 2022; Banerjee et al. 2023; Tiwari et al. 2024). After defining the effective Hubble parameters through the expansion rate of  $\Lambda\text{CDM}$  and  $w\text{CDM}$  models, Montani et al. (2025) and Jia et al. (2025a) proposed that a running  $H_0$  naturally arises from evolving dark energy. Because phantom-crossing behavior can drive a faster expansion phase leading to large  $H_0$ , the concept of an evolved  $H_0(z)$  is theoretically motivated. Furthermore, our reconstructions of  $w(z)$  are compatible with various dynamical dark-energy models. If dark energy can possess multiple internal degrees of freedom, such as multi-field models (Hu

2005; Guo et al. 2005; Cai et al. 2008), modified vacuum models (Parker & Raval 2000; Caldwell et al. 2006), and interacting dark-energy models (Billyard & Coley 2000), phantom crossing can be generated properly.

Beyond traditional approaches, many novel astrophysical probes covering a broad range of redshift have been proposed to measure the cosmological parameters and the dark-energy EoS. For instance, the spectral peak of gamma-ray burst (merger events via gravitational-wave observations) can serve as a tracer (standard sirens) of cosmic expansion (Dai et al. 2004; Abbott et al. 2017; Wang et al. 2023; Li et al. 2024), the dispersion measures of fast radio bursts provide independent constraints on  $H_0$  and  $w(z)$  (Zhou et al. 2014; Wang et al. 2025), and the propagation speed of gravitational waves from multi-messenger events can test large classes of scalar-tensor and dark-energy theories (Ezquiaga & Zumalacárregui 2017). In addition to  $w(z)$  and  $H_0$ , several other cosmological parameters have been modeled as redshift-dependent functions to explain current cosmological tensions (Ó Colgáin et al. 2022; Fazzari et al. 2026; Ó Colgáin et al. 2024). Looking forward, next-generation CMB experiments (CMB-S4, the Simons Observatory, and LiteBIRD) (Abazajian et al. 2022; Lee et al. 2019; LiteBIRD Collaboration et al. 2023), together with high-precision BAO surveys such as Euclid (Euclid Collaboration et al. 2025), will substantially tighten cosmological constraints and provide crucial insights into the physics of dark energy and cosmic expansion.

**Acknowledgements.** We thank the anonymous referee for helpful comments and suggestions. This work is supported in part by NSFC under grants of No. 12233011, the Postdoctoral Fellowship Program of CPSF (No. GZB20250738), and the Jiangsu Funding Program for Excellent Postdoctoral Talent (No. 2025ZB209).

## References

Abazajian, K., Abdulghafour, A., Addison, G. E., Adshead, P., et al. 2022, arXiv e-prints, arXiv:2203.08024

Abbott, B. P., Abbott, R., Abbott, T. D., et al. 2017, *Nature*, 551, 85

Abdalla, E., Abellán, G. F., Abourahim, A., et al. 2022, *Journal of High Energy Astrophysics*, 34, 49

Abedin, M., Wang, G.-J., Ma, Y.-Z., & Pan, S. 2025, *MNRAS*, 540, 2253

Armendariz-Picon, C., Mukhanov, V., & Steinhardt, P. J. 2000, *Phys. Rev. Lett.*, 85, 4438

Banerjee, S., Petronikolou, M., & Saridakis, E. N. 2023, *Phys. Rev. D*, 108, 024012

Benevento, G., Hu, W., & Raveri, M. 2020, *Phys. Rev. D*, 101, 103517

Billyard, A. P. & Coley, A. A. 2000, *Phys. Rev. D*, 61, 083503

Brieden, S., Gil-Marín, H., & Verde, L. 2023, *J. Cosmology Astropart. Phys.*, 2023, 023

Brout, D., Scolnic, D., Popovic, B., et al. 2022, *ApJ*, 938, 110

Buchner, J. 2016, PyMultiNest: Python interface for MultiNest, *Astrophysics Source Code Library*, record ascl:1606.005

Cai, Y.-F., Qiu, T., Brandenberger, R., Piao, Y.-S., & Zhang, X. 2008, *J. Cosmology Astropart. Phys.*, 2008, 013

Caldwell, R. R. 2002, *Physics Letters B*, 545, 23

Caldwell, R. R., Komp, W., Parker, L., & Vanzella, D. A. T. 2006, *Phys. Rev. D*, 73, 023513

Dai, Z. G., Liang, E. W., & Xu, D. 2004, *ApJ*, 612, L101

Dainotti, M. G., De Simone, B., Garg, A., et al. 2025, *Journal of High Energy Astrophysics*, 48, 100405

Dainotti, M. G., De Simone, B., Schiavone, T., et al. 2021, *ApJ*, 912, 150

Dainotti, M. G., De Simone, B. D., Schiavone, T., et al. 2022, *Galaxies*, 10, 24

DES Collaboration, Abbott, T. M. C., Acevedo, M., et al. 2024, *ApJ*, 973, L14

DESI Collaboration, Abdul-Karim, M., Aguilar, J., et al. 2025, *Phys. Rev. D*, 112, 083515

Di Valentino, E. & Brout Dillon. 2024, The Hubble Constant Tension

Di Valentino, E., Mukherjee, A., & Sen, A. A. 2021, *Entropy*, 23, 404

Di Valentino, E., Said, J. L., Riess, A., et al. 2025, *Physics of the Dark Universe*, 49, 101965

Euclid Collaboration, Mellier, Y., Abdurro'uf, Acevedo Barroso, J. A., et al. 2025, *A&A*, 697, A1

Ezquiaga, J. M. & Zumalacárregui, M. 2017, *Phys. Rev. Lett.*, 119, 251304

Fazzari, E., Giarè, W., & Di Valentino, E. 2026, *ApJ*, 996, L5

Feng, B., Li, M., Piao, Y.-S., & Zhang, X. 2006, *Physics Letters B*, 634, 101

Feng, B., Wang, X., & Zhang, X. 2005, *Physics Letters B*, 607, 35

Giarè, W. 2025, *Phys. Rev. D*, 112, 023508

Goldstein, S., Celoria, M., & Schmidt, F. 2025, arXiv e-prints, arXiv:2507.16970

Gu, G., Wang, X., Wang, Y., et al. 2025, *Nature Astronomy*

Guo, Z.-K., Piao, Y.-S., Zhang, X., & Zhang, Y.-Z. 2005, *Physics Letters B*, 608, 177

Holsclaw, T., Alam, U., Sansó, B., et al. 2010, *Phys. Rev. Lett.*, 105, 241302

Horndeski, G. W. 1974, *International Journal of Theoretical Physics*, 10, 363

Hu, W. 2005, *Phys. Rev. D*, 71, 047301

Jeffreys, H. 1939, *Theory of Probability*

Jia, X. D., Hu, J. P., Gao, D. H., Yi, S. X., & Wang, F. Y. 2025a, *ApJ*, 994, L22

Jia, X. D., Hu, J. P., Yi, S. X., & Wang, F. Y. 2025b, *ApJ*, 979, L34

Krishnan, C., Colgáin, E. O., Ruchika, et al. 2020, *Phys. Rev. D*, 102, 103525

Krishnan, C., Ó Colgáin, E., Sheikh-Jabbari, M. M., & Yang, T. 2021, *Phys. Rev. D*, 103, 103509

Lee, A., Abitbol, M. H., Adachi, S., Ade, P., et al. 2019, in *Bulletin of the American Astronomical Society*, Vol. 51, 147

Lee, B.-H., Lee, W., Ó Colgáin, E., Sheikh-Jabbari, M. M., & Thakur, S. 2022, *J. Cosmology Astropart. Phys.*, 2022, 004

Li, Y.-J., Tang, S.-P., Wang, Y.-Z., & Fan, Y.-Z. 2024, *ApJ*, 976, 153

Li, Y.-J., Wang, Y.-Z., Han, M.-Z., et al. 2021, *ApJ*, 917, 33

LiteBIRD Collaboration, Ally, E., Arnold, K., et al. 2023, *Progress of Theoretical and Experimental Physics*, 2023, 042F01

Lodha, K., Calderon, R., Matthewson, W. L., et al. 2025, *Phys. Rev. D*, 112, 083511

Lopez-Hernandez, M. & De-Santiago, J. 2025, *J. Cosmology Astropart. Phys.*, 2025, 026

Malekjani, M., Mc Conville, R., Ó Colgáin, E., Pourojaghi, S., & Sheikh-Jabbari, M. M. 2024, *European Physical Journal C*, 84, 317

Montani, G., Carlevaro, N., & Dainotti, M. G. 2025, *Physics of the Dark Universe*, 48, 101847

Ó Colgáin, E. & Sheikh-Jabbari, M. M. 2025, *MNRAS*, 542, L24

Ó Colgáin, E., Sheikh-Jabbari, M. M., Solomon, R., et al. 2022, *Phys. Rev. D*, 106, L041301

Ó Colgáin, E., Sheikh-Jabbari, M. M., Solomon, R., Dainotti, M. G., & Stojkovic, D. 2024, *Physics of the Dark Universe*, 44, 101464

Pang, Y.-H., Zhang, X., & Huang, Q.-G. 2025, *Science China Physics, Mechanics, and Astronomy*, 68, 280410

Parker, L. & Raval, A. 2000, *Phys. Rev. D*, 62, 083503

Perivolaropoulos, L. & Skara, F. 2022, *New Astronomy Reviews*, 95, 101659

Petronikolou, M., Basilakos, S., & Saridakis, E. N. 2022, *Phys. Rev. D*, 106, 124051

Planck Collaboration, Aghanim, N., Akrami, Y., et al. 2020, *A&A*, 641, A6

Ratra, B. & Peebles, P. J. E. 1988, *Phys. Rev. D*, 37, 3406

Raveri, M., Bull, P., Silvestri, A., & Pogosian, L. 2017, *Phys. Rev. D*, 96, 083509

Riess, A. G., Casertano, S., Yuan, W., et al. 2021, *ApJ*, 908, L6

Riess, A. G., Li, S., Anand, G. S., et al. 2025, *ApJ*, 992, L34

Riess, A. G., Yuan, W., Macri, L. M., et al. 2022, *ApJ*, 934, L7

Rubin, D., Aldering, G., Betoule, M., et al. 2025, *ApJ*, 986, 231

Scherer, M., Sabogal, M. A., Nunes, R. C., & De Felice, A. 2025, *Phys. Rev. D*, 112, 043513

Schöneberg, N. 2024, *J. Cosmology Astropart. Phys.*, 2024, 006

Scolnic, D., Brout, D., Carr, A., et al. 2022, *ApJ*, 938, 113

Shafieloo, A., Kim, A. G., & Linder, E. V. 2012, *Phys. Rev. D*, 85, 123530

Tiwari, Y., Ghosh, B., & Jain, R. K. 2024, *European Physical Journal C*, 84, 220

Wang, Y.-Y., Gao, S.-J., & Fan, Y.-Z. 2025, *ApJ*, 981, 9

Wang, Y.-Y., Lei, L., Tang, S.-P., & Fan, Y.-Z. 2026, *J. Cosmology Astropart. Phys.*, 2026, 009

Wang, Y.-Y., Tang, S.-P., Jin, Z.-P., & Fan, Y.-Z. 2023, *ApJ*, 943, 13

Wong, K. C., Suyu, S. H., Chen, G. C. F., et al. 2020, *MNRAS*, 498, 1420

Zhao, G.-B., Crittenden, R. G., Pogosian, L., & Zhang, X. 2012, *Phys. Rev. Lett.*, 109, 171301

Zhao, G.-B., Raveri, M., Pogosian, L., et al. 2017, *Nature Astronomy*, 1, 627

Zhou, B., Li, X., Wang, T., Fan, Y.-Z., & Wei, D.-M. 2014, *Phys. Rev. D*, 89, 107303

## Appendix A: The results of parameter estimations for various cosmological models

This appendix presents the posterior distributions of the cosmological parameters and the corresponding Bayesian evidences for all scenarios discussed in the main text. For the reconstructions of  $H_0(z)$ , we show the values at  $z \sim 0.01$  and  $z \sim 0.36$ . For  $w(z)$ , the specific and local extreme values are listed.

Posterior distributions in 68% credible intervals for multi cases

Datasets	Cases	$H_0(z \sim 0.01) H_0(z \sim 2.35) w(z \sim 0.01) w(z \sim 0.62) w(z \sim 1.02) w(z \sim 1.52) w(z \sim 2.35)$	$\Omega_m$	$\Omega_b h^2$	$\ln(E)$
		(km s <sup>-1</sup> Mpc <sup>-1</sup> )			
D+P	M	73.12 <sup>+0.91</sup> <sub>-0.85</sub>	71.46 <sup>+1.31</sup> <sub>-1.35</sub>	0.15 <sup>+1.23</sup> <sub>-1.16</sub>	-1.20 <sup>+0.17</sup> <sub>-0.17</sub>
	G	73.11 <sup>+0.90</sup> <sub>-0.85</sub>	71.60 <sup>+1.27</sup> <sub>-1.26</sub>	0.29 <sup>+1.61</sup> <sub>-1.45</sub>	-1.20 <sup>+0.12</sup> <sub>-0.12</sub>
	H	73.27 <sup>+0.85</sup> <sub>-0.88</sub>	70.78 <sup>+0.95</sup> <sub>-0.98</sub>	-1.82 <sup>+0.68</sup> <sub>-0.69</sub>	-1.39 <sup>+0.29</sup> <sub>-0.28</sub>
	$w$ CDM	72.18 <sup>+0.77</sup> <sub>-0.79</sub>	-	-0.96 <sup>+0.03</sup> <sub>-0.03</sub>	-
	$\Lambda$ CDM	72.77 <sup>+0.54</sup> <sub>-0.55</sub>	-	-	-
	$w$ QCDM	71.33 <sup>+2.59</sup> <sub>-2.61</sub>	69.53 <sup>+1.48</sup> <sub>-1.38</sub>	0.08 <sup>+1.36</sup> <sub>-1.11</sub>	-1.17 <sup>+0.18</sup> <sub>-0.17</sub>
D+D	M	71.62 <sup>+2.54</sup> <sub>-2.58</sub>	69.59 <sup>+1.47</sup> <sub>-1.35</sub>	0.55 <sup>+1.41</sup> <sub>-1.44</sub>	-1.14 <sup>+0.14</sup> <sub>-0.12</sub>
	G	75.81 <sup>+2.53</sup> <sub>-3.39</sub>	67.41 <sup>+1.36</sup> <sub>-1.13</sub>	-2.28 <sup>+0.84</sup> <sub>-0.92</sub>	-1.36 <sup>+0.32</sup> <sub>-0.30</sub>
	H	68.42 <sup>+1.21</sup> <sub>-1.23</sub>	-	-0.84 <sup>+0.04</sup> <sub>-0.04</sub>	-
	$w$ CDM	72.24 <sup>+0.66</sup> <sub>-0.66</sub>	-	-	-
	$\Lambda$ CDM	71.36 <sup>+2.03</sup> <sub>-2.01</sub>	0.33 <sup>+1.54</sup> <sub>-1.55</sub>	-1.78 <sup>+0.41</sup> <sub>-0.40</sub>	-0.31 <sup>+0.36</sup> <sub>-0.36</sub>
	$w$ QCDM	74.05 <sup>+2.80</sup> <sub>-2.82</sub>	71.79 <sup>+2.52</sup> <sub>-3.35</sub>	-0.29 <sup>+1.93</sup> <sub>-2.00</sub>	-2.39 <sup>+0.80</sup> <sub>-0.78</sub>
D+U	M	76.29 <sup>+3.38</sup> <sub>-3.35</sub>	68.38 <sup>+1.75</sup> <sub>-1.49</sub>	-2.07 <sup>+0.84</sup> <sub>-0.94</sub>	-1.60 <sup>+0.30</sup> <sub>-0.30</sub>
	G	75.51 <sup>+2.90</sup> <sub>-3.51</sub>	-	-0.86 <sup>+0.05</sup> <sub>-0.05</sub>	-
	H	69.12 <sup>+1.43</sup> <sub>-1.47</sub>	-	-	-
	$w$ CDM	72.32 <sup>+0.66</sup> <sub>-0.67</sub>	-	-	-
	$\Lambda$ CDM	-	-	-	-

Table A.1: ‘D+P’, ‘D+D’, and ‘D+U’ represents the data combinations of DESI + Pantheon, DESI + DESY5, and DESI + Union, respectively. ‘M’, ‘G’, and ‘U’ represent the cases that the priors of  $w(z)$  are derived using the Matérn-3/2 kernel, the Gaussian kernels, and the Hornedeski theory.  $\ln(E)$  denotes the Bayesian evidence corresponding to each case.